Porous Substrates for Label-Free Molecular Level Detection of Nonresonant Organic Molecules

Hyunhyub Ko,[†] Sehoon Chang, and Vladimir V. Tsukruk*

School of Materials Science and Engineering and School of Polymer, Textile, and Fiber Engineering, Georgia Institute of Technology, Atlanta, Georgia 30332. [†]Current address: Department of Electrical Engineering and Computer Sciences, University of California at Berkeley, Berkeley, CA 94720.

ABSTRACT We report on the design of practical surface enhanced Raman scattering (SERS) substrate based upon 3D alumina membranes with cylindrical nanopores chemically modified with polyelectrolyte coating and loaded with gold nanoparticle clusters. These substrates allow for a molecular-level, label-free detection of common plastic explosive materials (TNT, DNT) down to 5—10 zeptograms or 15—30 molecules and a common liquid explosive (HMTD) down to 1 picogram. Such a sensitive detection of organic molecules by utilizing efficient SERS substrates opens the path for affordable and label-free detection of trace amount of practically important chemical compounds.

KEYWORDS: surface enhanced Raman scattering (SERS) · explosives detection · nanoporous structures · gold nanoparticles

Since the demonstration of single molecule detection,[1,2] surface-enhanced Raman scattering (SERS) has emerged as one of prospective sensing tools for highly sensitive detection of trace chemicals.[3,4] The capability of trace level detection is due to the Raman signal enhancement by the large electromagnetic fields on the small gaps between metal nanoparticles, which are also known as "hot spots".[5] To date, numerous designs of SERS media such as metal nanoparticle films[6−8] and metallic nanostructures[9−12] have been suggested. Modest additional enhancement has been achieved by using optical waveguiding properties for photonic crystal fibers with a limited range of dimensions.[13,14] Three-dimensional (3D) nanoporous alumina membranes (PAMs) with vertical cylindrical nanopores showed high SERS activity (Figure 1).[15] It is suggested that the significantly enhanced Raman scattering is related to the optical waveguide effect in addition to the large specific surface area, large diameter, and optical transparency with minimal light absorption.[16,17] However, single molecule or near-molecular detection with conventional SERS substrates have been demonstrated only for some molecules labeled with Raman markers and very few selected model compounds with highly resonant chemical structures such as, for example, rhodamine 6G and crystal violet showing combined electromagnetic and chemical enhancement as high as 10^{14}.[18−20]

Such a restriction limits the usefulness of SERS technique for the detection of important organic compounds without extensive resonating chemical structures such as known plastic and liquid explosives based on nitrotoluenes (TNT, DNT) and peroxides (TATP, HMTD).[4] Indeed, direct comparison of SERS enhancement for rhodamine 6G and DNT showed that the enhancement of the later compound is 4 orders of magnitude lower, which, essentially, prevents any molecular-level detection on conventional SERS substrates suggested to date.[21] In fact, despite significant efforts, these classes of compounds usually remain "stealthy" in Raman measurements. For example, the lowest limit of detection reported in literature for DNT is few parts per billion (ppb) in the solid state on metal nanostructured substrates [21−23] and hundredths of μM in solution,[24] a modest level far from single molecule ability demonstrated for Raman markers such as rhodamine 6G and crystal violet.

Herein, we report on the design of SERS-active ordered porous substrates allowing for a label-free, near-molecular level of detection of explosive organic compounds, 2,4-dinitrotoluene (DNT) and trinitrotoulene (TNT), down to 0.1−0.05 ppt which is more than 4 orders of magnitude better than that previously reported (1 ppb).[23] The total amount of the detected material precipitated on substrates is 5−10 zeptograms (in contrast to 1 pg in previous studies[23]),

*Address correspondence to vladimir@mse.gatech.edu.

Received for review September 10, 2008 and accepted December 03, 2008.

Published online December 15, 2008.
10.1021/nn800569f CCC: $40.75

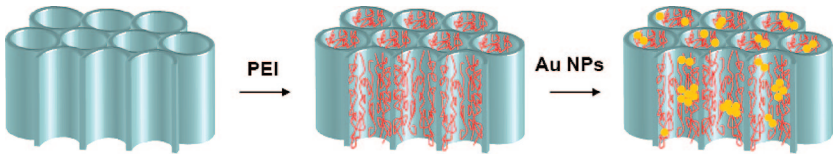

Figure 1. Fabrication procedures for 3D nanoporous membranes decorated with aggregated gold nanoparticle clusters. The surface of porous alumina membranes are functionalized with positively charged amine-groups by modification with PEI, and CTAB-capped gold colloids are then passed through the PEI-modified porous alumina membranes resulting in the formation of aggregated gold nanoparticle clusters inside the pores.

which is an equivalent of 15−30 molecules within the laser beam (Figure 1) cross-section (30 μm in a diameter). High detection sensitivity was demonstrated for peroxide explosive as well. We achieved this unprecedented detection limit for nonlabeled small nonresonating molecules by utilizing "hot spots" of nanoparticle clusters within chemically modified nanoporous alumina membranes transparent for laser beam (Figure 2). For the cluster-loaded nanoporous substrates suggested here we observed outstanding SERS enhancement which is much higher (over 6 orders of magnitude) than that reported in our previous work on alumina membranes decorated with individual nanoparticles.[15]

RESULTS AND DISCUSSION

Figure 1 shows the fabrication routine for controlled assembly of nanoparticle aggregates inside the porous alumina membranes. A critical step in fabrication efficient SERS substrates was the assembling of the proper concentration of gold nanoparticle clusters on the inner walls of cylindrical nanopores. Generally, the assembly of nanoparticle clusters on the inner-walls of nanopores is not easily achievable because the relatively large and metastable nanoparticle clusters cannot easily go into the nanopores and attach on the alumina surface. To overcome this problem, we utilized electrostatic interaction between the charged gold nanoparticles and the properly charged polyelectrolyte-modified alumina surface to control nanoparticle aggregations on the modified inner surfaces. For this purpose, the surface of porous alumina membranes was modified with polyethylenimine (PEI), where columbic repulsions between positively charged PEI and gold nanoparticles prevents the attachment of gold nanoparticles on the outer-surface of alumina membranes, which often cause the pore-blocking. The amine groups in the PEI, on the other hand, are used to attach gold nanoparticles on the inner walls of porous alumina membranes by partial replacement with the cetyltrimethylammonium bromide (CTAB) ligands on the gold nanoparticle surface during the filtration of gold nanoparticle solution.

The CTAB ligand plays a major role in the controlled aggregation level inside the pores stabilizing nanoparticles by repulsive forces.[25] For certain concentration, the CTAB molecules are known to link together the {100} facets of neighboring gold nanoparticles, assembling them into linear chains.[26,27] Moreover, CTAB bilayers create "soft shell" around nanoparticles with the thickness of about 2 nm and such aggregates are considered to be ideal for "hot spots" with strong SERS effect, an approach well-known for nanoparticle assemblies on planar SERS substrates.[5] We found that the gold nanoparticles can be assembled as small clusters on the inner walls of nanopores by optimizing the concentration of CTAB within 1−10 μM. The CTAB concentration over or below the optimum values results in either very concentrated tethered nanoparticles or their preferential attachment only on the outer surface of membranes.

Loading with gold nanoparticle aggregates results in a membrane color change to purple-blue (Figure 2a). These clusters on the inner walls of cylindrical nanopores are easily observed on a fractured membrane with SEM (Figure 2b). As can be seen from high resolution SEM images most of gold nanoparticles are tethered onto the pore walls as clusters with different aggregation numbers (Figure 3a,b). Overall, about 50% of all nanoparticles aggregated into dimers and trimers under given conditions as can be concluded from direct counting of nanoparticles on SEM images (see histogram of aggregation number distribution in Figure 3c). Similar behavior of the nanoparticle with their assembly into linear chains of dimers or trimers has been reported previously for similar polyelectrolyte surfaces in the course of electrostatically driven adsorption or on silica surfaces by controlling the concentration of CTAB within 0.25−1 μM. [26,28]

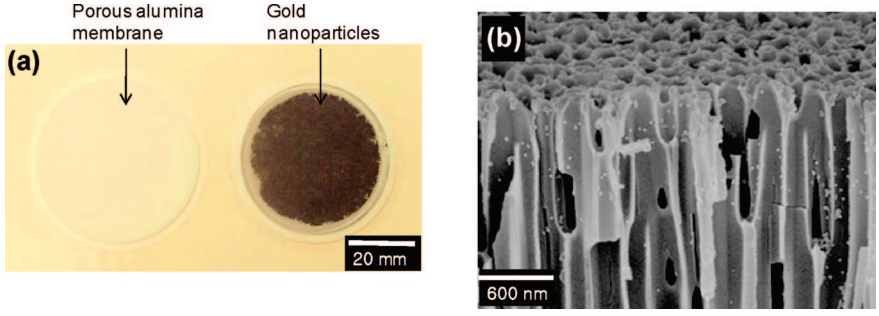

Figure 2. (a) Photograph of porous alumina membranes before (left) and after (right) the loading with gold nanoparticles; (b) SEM image of fractured membrane loaded with gold nanoparticle clusters.

The Raman spectra of high concentration DNT on 3D SERS substrate is characterized by two strong bands assigned to vibration modes of NO_2 groups at 834 cm^{-1} for NO_2 out-of-plane bending (ρ_{NO2}) and 1342 cm^{-1} for NO_2 stretching (ν_{NO2}) (Figure

4a).[29−31] The signature stretching mode at 1342 cm^{-1} was utilized to detect the presence of DNT compound in a wide range of concentration from 50 mM down to a trace amount (Figure 4b). As was observed, the peak intensity increases sharply at higher concentrations and reached saturation (Figure 5a). A sharp peak at 1342 cm^{-1} is clearly visible down to 100 ppt (Figure 4b).

The intensity of NO_2 stretching band increased steady with increasing DNT concentration (Figure 5). At higher concentration, the increase in the intensity of this Raman band saturates above 4 mM due to full occupation of adsorption sites by the DNT molecules. It is worth noting that this saturation concentration of analyte is much higher than typical planar substrates, providing a much larger dynamic range of detection, another important advantage of 3D substrate suggested here.

The adsorption isotherm obtained here for the DNT compound can be fit by parabolic function in semilog coordinates which corresponds to Frumkin adsorption behavior. [32,33] Fitting the experimental adsorption data with the Frumkin expression, $\ln[\theta/C(1-\theta)] = 2g\theta + \ln K$, where θ is the fractional coverage taken as a ratio $I_{1343}/I_{1343max}$; C is the DNT solution concentration; g is Frumkin parameter; K is the adsorption constant of DNT, which gives a value of $K = 1.21 \times 10^4\ M^{-1}$. This large value indicates the strong interaction between the adsorbing DNT molecules with electron-deficient NO_2 groups and the PEI-modified inner walls with electron-rich amine groups.

To estimate the lowest detectable amount, the Raman band in this wave range was treated by subtracting background, smoothing, averaging several independent spectra from different locations, and conducting Gaussian fitting without fixing peak positions (see several examples of fitting in Figure 6). The best fitting was obtained with four peaks. Three of them at 1355, 1367, and 1382 cm^{-1} with virtually unchanged positions can be assigned to CH_2 wagging vibrations of PEI matrix and CTAB molecules (Figures 6 and 7).[34,35] The last peak which corresponds to a characteristic NO_2 stretching band, showed at unchanged position, 1342 ± 2 cm^{-1} at all concentrations (Figure 7).

From our data, the lowest detectable concentration in solution is 0.1 ppt as determined by utilizing a standard definition of signal-to-noise (S/N) ratio of 3:1. A noise level was determined as an average standard deviation in given wavenumber region and its value was directly compared with the intensity of the individual peaks obtained from the fitting procedure (Figure 6).

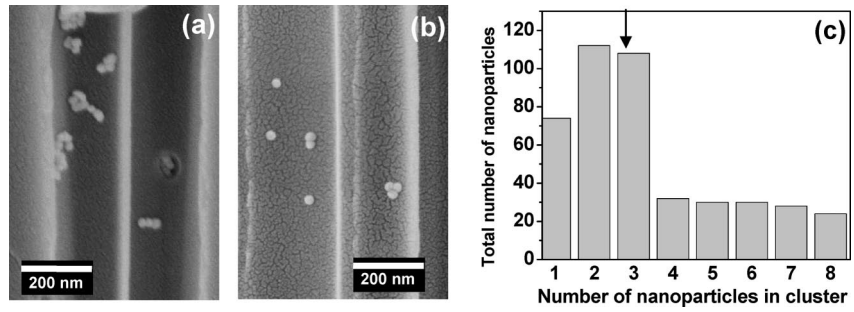

Figure 3. (a,b) High-resolution SEM images of gold nanoparticle clusters inside the cylindrical pores; (c) histogram of the aggregation numbers of gold nanoparticles inside the pores; the average value is indicated by an arrow.

This unprecedently low detection limit corresponds to 10 zeptograms of DNT material within the interrogated area (30 μm diameter laser spot), which is about 30 DNT molecules. This value indicates molecular-level detection, a phenomenon demonstrated only for a few model resonance-enhanced Raman markers. Moreover, the amount detected here is eight orders of magnitude below the conventional detection limit of DNT amount claimed in literature (1 pg) on planar SERS substrates such as roughened metal surfaces.[23] Besides, DNT vapor detection was preliminary demonstrated as well with a low limit of detection below 100 ppt, hence indicating that the design suggested here is also applicable to efficient detection of vapor phase, usually the most difficult task to perform.

The enhancement factor was estimated for this combination of substrate−compound by using a reference sample according to a usual approach adapted in the literature.[36,37] Briefly, the SERS peak intensity of DNT at 1342 cm^{-1} was compared with the normal Raman peak intensity of reference DNT film of the known thickness and the SERS enhancement factor (EF) was calculated by using the following equation: $EF = I_{SERS}/I_{ref} \times$ [reference]/[SERS], where I_{SERS} and I_{ref} are the measured Raman intensities and [SERS] and [reference] are the concentrations of target molecules in the SERS and

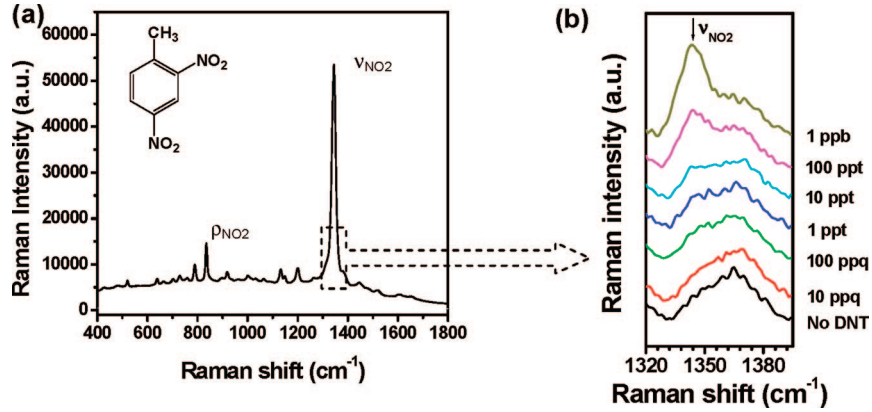

Figure 4. (a) Raman spectrum of 10000 ppm 2,4-DNT on SERS substrate. The inset shows the chemical structure of 2,4-DNT. (b) Raman spectra of trace level 2,4-DNT on SERS substrate in the window of the strongest NO_2 stretching vibration.

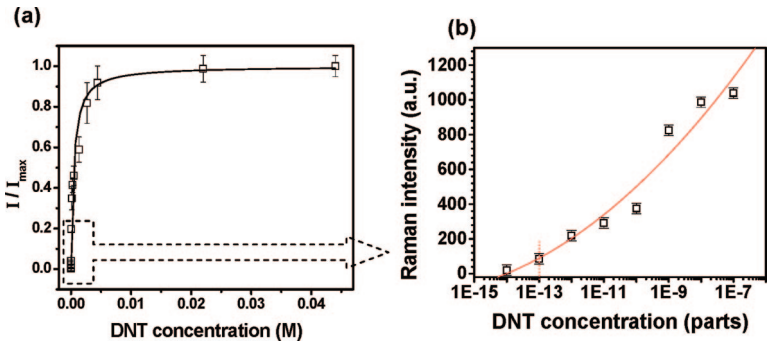

Figure 5. (a) Overall intensity at 1342 cm^{-1} for different concentrations of DNT compound; (b) intensity at 1342 cm^{-1} for trace level concentrations of DNT compound expressed in parts (from 100 ppb and down to 10 ppq). Here and in the text parts are expressed in weight fractions.

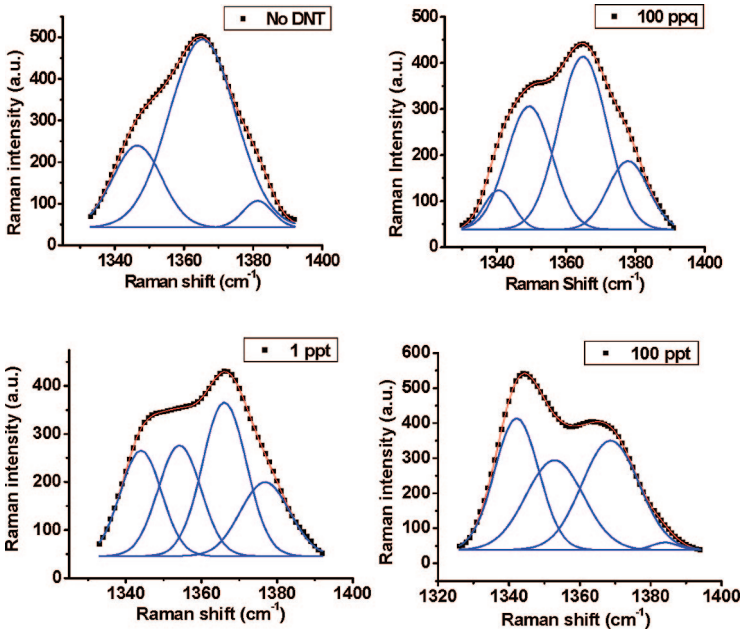

Figure 6. Gaussian fitting of Raman bands for different DNT concentrations.

reference samples, respectively. The value obtained is extremely high, within $10^{12}-10^{13}$, which is close to the record enhancement of 10^{14} reported for large, resonant molecules. [18] This Raman enhancement was about 10^{10} times higher than that of gold nanoparticles on planar substrates with similar surface density.[15] From comparison with previous results, we can estimate that the total Raman enhancement of $10^{12}-10^{13}$ might be ascribed to the $10^{6}-10^{7}$ times contribution by "hot" nanoparticle clusters and $10^{5}-10^{6}$ "additional" enhancement. This additional contribution might be caused by large specific surface area (3×10^{2} times) of porous alumina membrane combined with the optical waveguide effect ($\sim 10^{3}$ times).[15]

This exceptional Raman enhancement by the optical waveguide effect can be explained by the increasing photon density of states caused by multiple total internal reflections at the pore air-alumina interface similarly to those reported for optical microcavities with cylindrical resonators,[38,39] transparent nanowires with diameter well below wavelength,[40] and nanoribbon waveguides.[41] In fact, for transparent alumina walls with the thickness of 47 $\pm$ 2 nm, the total internal reflection at the alumina−air interface occurs at the angle of incidence above the critical angle, $\theta = 38°$, (with respect to the normal to the interface, $\sin\theta = n_{air}/n_{alumina}$; n is corresponding refractive index at 785 nm). Thus, we can roughly estimate that the "bouncing" of light trapped within PAM walls from the opposite interface should occur every ~40 nm along the cylindrical pore. Hence, about 3×10^{3} multiple internal reflections occur for light passing through walls of 60 μm membrane and reflecting from silicon substrate (overall transmittance is about 50%, see below). This rough estimate agrees with our experimental observation ($\sim 10^{3}$ additional contribution) and supports our suggestion of optical waveguiding effect as a major contributor to the strong Raman enhancement observed here.

Since the metal nanoparticles attached on the waveguide surface can intensely scatter and attenuate waveguided light, we tested the absorption, transmission, and SERS intensity variation with nanoparticle loading to see the effects of light propagation and therefore multiple reflections through the waveguides. First, the change in light interaction with the 3D SERS substrates with the loading of gold nanoparticles can be clearly seen in the data for absorption and transmission of light in Figure 8a. The bare porous alumina membranes show no obvious absorption peaks in this range. When the gold nanoparticles are infiltrated into the membranes, a strong band at 530 nm and weak band at 600−800 nm appear. The band at shorter-wavelength is ascribed to the surface plasmon resonance of single gold nanoparticles. As the amount of gold nanoparticles inside the membranes increases, an increase in longer-wavelength band is evident (Figure

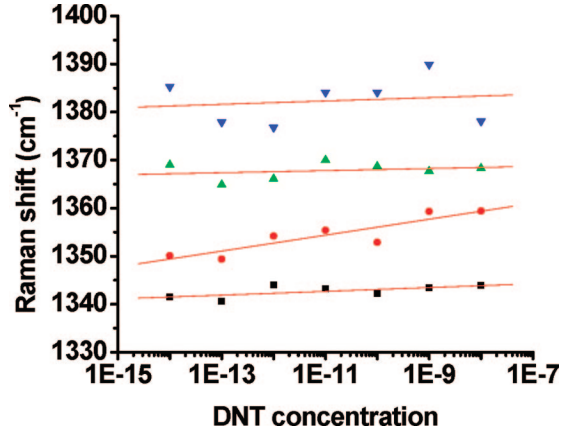

Figure 7. The variations of Raman band positions of four different peaks obtained from Gaussian fitting.

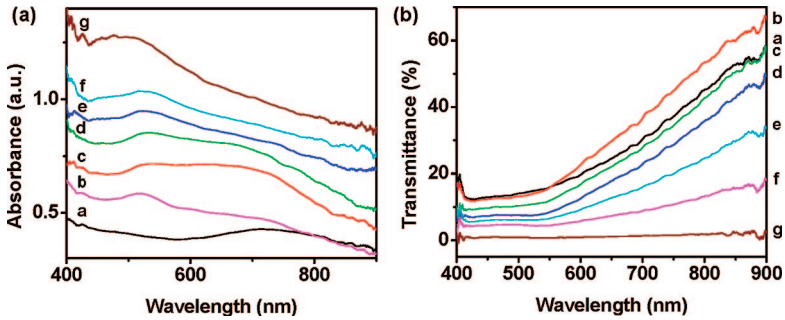

Figure 8. (a) Absorbance and (b) transmittance of porous membranes decorated with gold nanoparticle clusters with different loading amount (0, 8, 16, 32, 64, 128, and 256 μmol/cm³ from a to g).

8a). This increase in longer-wavelength indicates increased coupling of plasmon resonances of adjacent gold nanoparticles with increasing the amount of nanoparticles. The interparticle coupling results in plasmon resonance shift to longer wavelength from single particle plasmon resonance because of the dipole−dipole interaction between adjacent nanoparticles, resulting in the reduction of plasmon frequency.[42−44]

Correspondingly, the transmittance changes with increasing loading amount of nanoparticles (Figure 8b). The change in transmission is also closely related to the change in SERS intensity. The addition of gold nanoparticles into the alumina membranes causes the decrease in light transmission. The transmission of bare porous alumina membranes is relatively high (up to 50%) in the near-IR range and decreases in the visible range because of the high scattering. Upon the incorporation of gold nanoparticles, the transmission of the Au−PAMs decreases for higher concentrations mainly due to high adsorption of photons by the gold nanoparticles.

The absorption at longer-wavelength (600−800 nm) becomes weaker than that of shorter-wavelength (~530 nm) when the nanoparticle loading is over 32 μmol/cm³ and disappear at higher loading (over 128 μmol/cm³) (Figure 9). This change in absorption in combination with the transmission can be associated with the decrease in SERS intensity after the nanoparticle concentration of 32 μmol/cm³ (Figure 9). Similar behavior has been observed for 2D nanoparticle aggregates with SERS intensity decreased after a critical point with increasing the surface coverage of nanoparticles.[45−47] This decrease in SERS intensity for 2D nanoparticle films has been explained by comparing the extinction maximum and the excitation wavelength.[47] At initial stage, the SERS intensity increases with the increase of the surface coverage of nanoparticles as long as the wavelength of plasmon resonance is shorter than excitation wavelength. Then, the SERS intensity decreases with further deposition of nanoparticles when the extinction maximum is longer than the excitation wavelength. It has been known that the largest SERS enhancement occurs when the wavelength of plasmon resonance lies between the excitation laser and the scattered Raman wavelengths, resulting in resonance with the surface plasmons.[48]

To clarify if the approach suggested here can be expandable to other small organic molecules from a common explosive list, we conducted preliminary SERS experiments by exploiting common plastic explosive TNT and liquid peroxide explosive hexamethylene triperox-

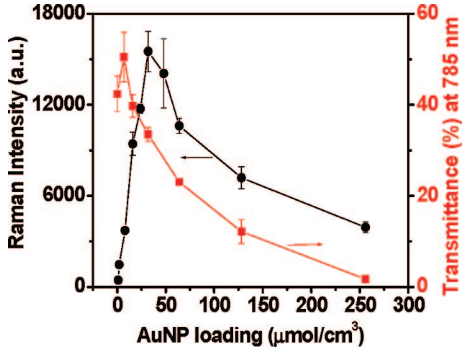

Figure 9. Comparison of Raman intensities at 1342 cm⁻¹ and transmittance at 785 nm wavelength for different loading levels.

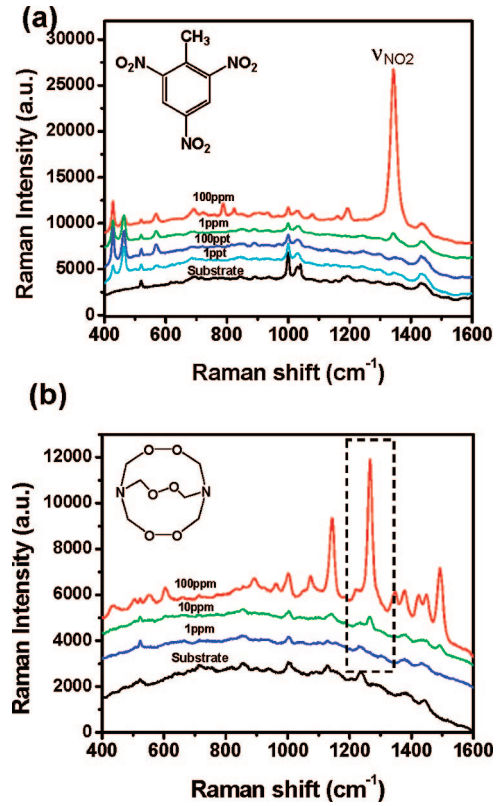

Figure 10. Raman spectra of TNT (a) and HMTD (b) on SERS substrates for different concentrations; characteristic signature peaks are marked; chemical formulas are inserted.

ide (HMTD) (Figure 10). The detection limit of TNT was calculated by comparing the relative Raman peak intensities of DNT and TNT recorded under identical loading conditions. Much stronger NO_2 vibration peak (up to two times higher) was detected for TNT molecules under identical experimental conditions, which facilitates an even lower detection limit close to 5 zeptograms or only 15 molecules within the laser footprint. We suggest that such an increase in SERS intensity in comparison with DNT is due to the presence of an additional NO_2 side group in TNT molecules.

Moreover, a trace level detection of peroxide explosives which are usually stealthy due to small Raman scattering cross-section[49] was achieved here for HMTD as well. In this case, we exploited 3D SERS chip decorated with gold nanorods and polyacrylonitrile matrix as will be discussed in detail elsewhere. An intense peak at 1266 cm^{-1} which is probably caused by local HMTD decomposition was tracked down to the concentration of the HMTD close to few ppms (Figure 10). The lowest detectable level achieved here corresponds to 1 pg of material within the interrogated area (30 μm diameter laser spot), which is more than 3 orders of magnitude better than the lowest limit of 1 ng detectable by desorption electrospray ionization.[50] It is worth noting that, to date, no trace SERS detection was demonstrated for this important class of molecules.

CONCLUSIONS

In conclusion, we realized a label-free, near-molecular level detection of explosive compounds down to 5−10 zeptograms or about 15−30 molecules of TNT and DNT. We achieved this outstanding detection limit by utilizing transparent porous membranes with cylindrical nanopores which provide means for waveguiding and multiple interactions of a laser beam passing through transparent walls with inner-wall surface decorated with "hot" gold nanoparticle clusters. The novelty of our design of SERS nanoporous substrate is in the utilization of gold nanoparticle clusters with optical waveguiding effects and high light transmission which all provide greatly increased interaction with finely tuned clusters of metal nanoparticles, which is different from planar substrates with "one-time" light-nanoparticle interaction events. On the other hand, virtually all previous SERS studies on metal nanoparticles (with few exceptions) in pores utilized just increased surface area of porous substrates without considering waveguiding or antenna properties which, as we estimated, adds 10^3 enhancement in Raman signal.[51−53]

Such a label-free, molecular level of detection of small nonresonant organic molecules from a broad class of plastic and liquid explosives with few active bonds by utilizing simple, large, and inexpensive nanoporous SERS substrates opens the path for affordable application of label-free SERS detection of trace amount of diverse classes of practically important chemical compounds ranging from chemical and biological agents and explosives to toxic environmental pollutants.

EXPERIMENTAL DETAILS

Porous alumina membranes (Anodisc 47, Whatman) were decorated with Au nanoparticles by filtration of Au nanoparticle solution on surface-modified 47 mm in diameter porous alumina membranes with cylindrical pore diameter of 243 ± 20 nm, wall thickness of 40 nm, and total thickness of 60 μm. Gold nanoparticles with diameter 32 nm and capped with CTAB were prepared by a seed growth method following the literature procedure.[54]

The immobilization of nanoparticles on porous alumina membranes was done by a modified literature procedure.[55,56] Here we loaded gold nanoparticle clusters by utilizing the electrostatically driven polyelectrolyte assembly inside cylindrical pores (Figure 1).[57] We utilized PEI for surface modification of inner walls and carefully tuned the concentration of CTAB to fabricate aggregated gold nanoparticles instead of individual gold nanoparticles inside the pores. Typically, the inner surface of porous membranes was modified with PEI (M_w = 55 000, Aldrich) by spin-casting (3000 rpm, 30 s) of 0.2% aqueous solution followed by rinsing with Nanopure water (18 MΩ cm), which results in 1−2 nm thick uniform PEI coating as has been demonstrated by AFM measurements in our previous work.[58] The concentration of CTAB was tuned by removing excess amounts of CTAB surfactant in the gold colloid solution *via* repeated centrifugation and multistep dilution.

For Raman testing, 10 μL of 2,4-DNT (Aldrich) solution in ethanol was drop-evaporated on SERS substrate with area of 1 cm^2 and kept to complete drying before SERS measurements. Concentration of DNT in solution was varied in a wide range by sequential dilution. Similar procedure was applied for other compounds studied here (TNT and HMTD) as well.

The Raman spectra were recorded by using a Holoprobe Raman microscope (Kaiser Optical Systems) with 10 × objective (NA = 0.25) and back-scattered configuration. The excitation laser (785 nm) power to the sample was 20 mW and collection time was 20 s. A field-emission scanning electron microscopy (FESEM, LEO 1530) was used to investigate the assembled structures of decorated membranes. A Leica fluorescent microscope with Creig spectrometer attachment has been used for the collection of UV−vis spectroscopic data in reflective and transmission modes.

Acknowledgment. We thank S. Singamaneni and Y.-H. Lee for useful discussion and technical assistance and M. Srinivasarao for use of Raman instrument. This work is supported by Army Research Office (ARO) and Air Force Office for Scientific Research (AFOSR).

REFERENCES AND NOTES

1. Nie, S. M.; Emory, S. R. Probing Single Molecules and Single Nanoparticles by Surface-Enhanced Raman Scattering. *Science* **1997**, *275*, 1102–1106.
2. Kneipp, K.; Wang, Y.; Kneipp, H.; Perelman, L. T.; Itzkan, I.; Dasari, R.; Feld, M. S. Single Molecule Detection Using Surface-Enhanced Raman Scattering (SERS). *Phys. Rev. Lett.* **1997**, *78*, 1667–1670.
3. Baker, G. A.; Moore, D. S. Progress in Plasmonic Engineering of Surface-Enhanced Raman-Scattering

Substrates Toward Ultra-Trace Analysis. *Anal. Bioanal. Chem.* **2005**, *382*, 1751–1770.
4. Moore, D. S. Instrumentation for Trace Detection of High Explosives. *Rev. Sci. Instrum.* **2004**, *75*, 2499–2512.
5. Kneipp, K.; Kneipp, H.; Kneipp, J. Surface-Enhanced Raman Scattering in Local Optical Fields of Silver and Gold Nanoaggregates—From Single-Molecule Raman Spectroscopy to Ultrasensitive Probing in Live Cells. *Acc. Chem. Res.* **2006**, *39*, 443–450.
6. Freeman, R. G.; Grabar, K. C.; Allison, K. J.; Bright, R. M.; Davis, J. A.; Guthrie, A. P.; Hommer, M. B.; Jackson, M. A.; Smith, P. C.; Walter, D. G.; *et al.* Self-Assembled Metal Colloid Monolayers: An Approach to SERS Substrates. *Science* **1995**, *267*, 1629–1632.
7. Wang, Z.; Pan, S.; Krauss, T. D.; Du, H.; Rothberg, L. J. The Structural Basis for Giant Enhancement Enabling Single-Molecule Raman Scattering. *Proc. Natl. Acad. Sci. U.S.A.* **2003**, *100*, 8638–8643.
8. Jiang, C.; Lio, W. Y.; Tsukruk, V. V. Surface Enhanced Raman Scattering Monitoring of Chain Alignment in Freely Suspended Nanomembranes. *Phys. Rev. Lett.* **2005**, *95*, 115503−1–4.
9. Hulteen, J. C.; Van Duyne, R. P. Nanosphere Lithography: A Materials General Fabrication Process for Periodic Particle Array Surfaces. *J. Vac. Sci. Technol., A* **1995**, *13*, 1553–1558.
10. Hulteen, J. C.; Treichel, D. A.; Smith, M. T.; Duval, M. L.; Jensen, T. R.; Van Duyne, R. P. Nanosphere Lithography: Size-Tunable Silver Nanoparticle and Surface Cluster Arrays. *J. Phys. Chem. B* **1999**, *103*, 3854–3863.
11. Gunawidjaja, R.; Peleshanko, S.; Ko, H.; Tsukruk, V. V. Bimetallic Nanocobs: Decorating Silver Nanowires with Gold Nanoparticles. *Adv. Mater.* **2008**, *20*, 1544–1549.
12. Qin, L.; Zhou, S.; Xue, C.; Atkinson, A.; Schatz, G. C.; Mirkin, C. A. Designing, Fabricating, and Imaging Raman Hot Spots. *Proc. Natl. Acad. Sci. U.S.A.* **2006**, *103*, 13300–13303.
13. Amezcua-Correa, A.; Yang, J.; Finlayson, C. E.; Peacock, A. C.; Hayes, J. R.; Sazio, P. J. A.; Baumberg, J. J.; Howdle, S. M. Surface-Enhanced Raman Scattering Using Microstructured Optical Fiber Substrates. *Adv. Funct. Mater.* **2007**, *17*, 2024–2030.
14. Yan, H.; Gu, C.; Yang, C.; Liu, J.; Jin, G.; Zhang, J.; Hou, L.; Yao, Y. Hollow Core Photonic Crystal Fiber Surface-Enhanced Raman Probe. *Appl. Phys. Lett.* **2006**, *89*, 204101–3.
15. Ko, H.; Tsukruk, V. V. Nanoparticle-Decorated Nanocanals for Surface-Enhanced Raman Scattering. *Small* **2008**, *4*, 1980–1984.
16. Saito, M.; Shibasaki, M.; Nakamura, S.; Miyagi, M. Optical Waveguides Fabricated in Anodic Alumina Films. *Opt. Lett.* **1994**, *19*, 710–712.
17. Lau, K. H. A.; Tan, S.; Tamada, K.; Sander, M. S.; Knoll, W. Highly Sensitive Detection of Processes Occurring Inside Nanoporous Anodic Alumina Templates: A Waveguide Optical Study. *J. Phys. Chem. B* **2004**, *108*, 10812–10818.
18. Homola, J. Surface Plasmon Resonance Sensors for Detection of Chemical and Biological Species. *Chem. Rev.* **2008**, *108*, 462–493.
19. McDonagh, C.; Burke, C. S.; MacCraith, D. D. Optical Chemical Sensors. *Chem. Rev.* **2008**, *108*, 400–422.
20. Ko, H.; Singamaneni, S.; Tsukruk, V. V. Nanostructured Surfaces and Assemblies as SERS Media. *Small* **2008**, *4*, 1576–1599.
21. Tao, A.; Kim, F.; Hess, C.; Goldberger, J.; He, R.; Sun, Y.; Xia, Y.; Yang, P. Langmuir-Blodgett Silver Nanowire Monolayers for Molecular Sensing Using Surface-Enhanced Raman Spectroscopy. *Nano Lett.* **2003**, *3*, 1229–1233.
22. Spencer, K. M.; Sylvia, J. M.; Marren, P. J.; Bertone, J. F.; Christesen, S. D. Surface-Enhanced Raman Spectroscopy for Homeland Defense. *Proc. SPIE* **2004**, *5269*, 1–8.
23. Spencer, K. M.; Sylvia, J. M.; Janni, J. A.; Klein, J. D. Advances in Land Mine Detection Using Surface-Enhanced Raman Spectroscopy. *Proc. SPIE* **1999**, *3710*, 373–379.
24. Cruz-Montoya, E. D. L.; Pérez-Acosta, G.; Pineda, T. L.; Hernández-Rivera, S. P. Surface Enhanced Raman Scattering of TNT and DNT on Colloidal Nanoparticles of Ag/TiO_2. *Proc. SPIE* **2007**, *6538*, 653826−1–10.
25. Nikoobakht, B.; Wang, Z. L.; El-Sayed, M. A. Self-Assembly of Gold Nanorods. *J. Phys. Chem. B* **2000**, *104*, 8635–8640.
26. Yang, Y.; Matsubara, S.; Nogami, M.; Shi, J.; Huang, W. One-Dimensional Self-Assembly of Gold Nanoparticles for Tunable Surface Plasmon Resonance Properties. *Nanotechnology* **2006**, *17*, 2821–2827.
27. Yang, Y.; Shi, J.; Tanaka, T.; Nogami, M. Self-Assembled Silver Nanochains for Surface-Enhanced Raman Scattering. *Langmuir* **2007**, *23*, 12042–12047.
28. Jiang, C.; Markutsya, S.; Pikus, Y.; Tsukruk, V. V. Freely Suspended Nanocomposite Membranes as Highly-Sensitive Sensors. *Nat. Mater.* **2004**, *3*, 721–728.
29. Ramos, C. M.; Alzate, L. F.; Colón, Y. M.; Santana, A.; Hernández, S. P.; Castro, M. E.; Briano, J. G.; Mina, N. Theoretical Studies of The Molecular Structures of Dinitrotoluenes and Their Interactions with Siloxane Surface of Clay Minerals. *Proc. SPIE* **2004**, *5415*, 1377–1388.
30. Blanco, A.; Mina, N.; Castro, M. E.; Castillo-Chará, J.; Hernández-Rivera, S. P. Effect of Environmental Conditions on the Spectroscopic Signature of DNT in Sand. *Proc. SPIE* **2005**, *5794*, 1281–1289.
31. Balaguera, M. D. L.; Montoya, E. D. L.; Castro, M. E.; Rivera-Montalvo, L. A.; Hernández-Rivera, S. P. Functionalization of Nitroexplosives for Surface-Enhanced Resonance Raman Spectroscopy of Silver Colloids. *Proc. SPIE* **2005**, *5778*, 327–336.
32. Volkova-Gugeshashvili, M. A.; Volkov, A. G.; Markin, V. S. Adsorption at Liquid Interfaces: The Generalized Frumkin Isotherm and Interfacial Structure. *Russ. J. Electrochemistry* **2006**, *42*, 1194–1200.
33. Mosier-Boss, P. A.; Lieberman, S. H. Detection of Anions by Normal Raman Spectroscopy and Surface-Enhanced Raman Spectroscopy of Cationic-Coated Substrates. *Appl. Spectrosc.* **2003**, *57*, 1129–1137.
34. Gailliez-Degremont, E.; Bacquet, M.; Laureyns, J.; Morcellet, M. Polyamines Adsorbed onto Silica Gel: A Raman Microprobe Analysis. *J. Appl. Polym. Sci.* **1997**, *65*, 871–882.
35. Dendramis, A. L.; Schwinn, E. W.; Sperline, R. P. A Surface-Enhanced Raman Scattering Study of CTAB Adsorption on Copper. *Surf. Sci.* **1983**, *13*, 675–688.
36. McFarland, A. D.; Young, M. A.; Dieringer, J. A.; Van Duyne, R. P. Wavelength Scanned Surface-Enhanced Raman Excitation Spectroscopy. *J. Phys. Chem. B* **2005**, *109*, 11279–11285.
37. Jackson, J. B.; Halas, N. J. Surface-Enhanced Raman Scattering on TunablePlasmonic Nanoparticle Substrates. *Proc. Natl. Acad. Sci. U.S.A.* **2004**, *101*, 17930–17935.
38. Kim, W.; Safonov, V. P.; Shalaev, V. M.; Armstrong, R. L. Fractals in Microcavities:Giant Coupled, Multiplicative Enhancement of Optical Responses. *Phys. Rev. Lett.* **1999**, *82*, 4811–4814.
39. White, I. M.; Oveys, H.; Fan, X. Increasing the Enhancement of SERS with Dielectric Microsphere Resonators. *Spectroscopy* **2006**, *21*, 36–42.
40. Tong, L; Gattass, R.; Ashcom, J. B.; He, S.; Lou, J.; Shen, M.; Maxwell, I.; Mazur, E. Subwavelength-Diameter Silica Wires for Low-Loss Optical Wave Guiding. *Nature* **2003**, *426*, 816–819.
41. Sirbuly, D. J.; Tao, A.; Law, M.; Fan, R.; Yang, P. Multifunctional Nanowire Evanescent Wave Optical Sensors. *Adv. Mater.* **2007**, *19*, 61–66.
42. Rechberger, W.; Hohenau, A.; Leitner, A.; Krenn, J. R.; Lamprecht, B.; Aussenegg, F. R. Optical Properties of Two Interacting Gold Nanoparticles. *Opt. Commun.* **2003**, *220*, 137–141.
43. Nikoobakht, B.; El-Sayed, M. A. Surface-Enhanced Raman Scattering Studies on Aggregated Gold Nanorods. *J. Phys. Chem. A* **2003**, *107*, 3372–3378.
44. Jain, P. K.; Huang, W.; El-Sayed, M. A. On the Universal Scaling Behavior of the Distance Decay of Plasmon Coupling in Metal Nanoparticle Pairs: A Plasmon Ruler Equation. *Nano Lett.* **2007**, *7*, 2080–2088.

45. Maxwell, D. J.; Emory, S. R.; Nie, S. Nanostructured Thin-Film Materials with Surface-Enhanced Optical Properties. *Chem. Mater.* **2001**, *13*, 1082–1088.
46. Adison, C. J.; Brolo, A. G. Nanoparticle-Containing Structures as a Substrate for Surface-Enhanced Raman Scattering. *Langmuir* **2006**, *22*, 8696–8702.
47. Olson, L. G.; Lo, Y.-S.; Beebe, T. P., Jr.; Harris, J. M. Characterization of Silane-Modified Immobilized Gold Colloids as a Substrate for Surface-Enhanced Raman Spectroscopy. *Anal. Chem.* **2001**, *73*, 4268–4276.
48. Haynes, C. L.; Van Duyne, R. P. Plasmon-Sampled Surface-Enhanced Raman Excitation Spectroscopy. *J. Phys. Chem. B* **2003**, *107*, 7426–7433.
49. Cotte-Rodríguez, I.; Chen, H.; Cooks, R. G. Rapid Trace Detection of Triacetone Triperoxide (TATP) by Complexation Reactions During Desorption Electrospray Ionization. *Chem. Commun.* **2006**, *9*, 953–955.
50. Cotte-Rodrýguez, I.; Hernandez-Soto, H.; Chen, H.; Cooks, R. G. In Situ Trace Detection of Peroxide Explosives by Desorption Electrospray Ionization and Desorption Atmospheric Pressure Chemical Ionization. *Anal. Chem.* **2008**, *80*, 1512–1519.
51. Williamson, T. L.; Guo, X.; Zukoski, A.; Sood, A.; Diaz, D. J.; Bohn, P. W. Porous GaN as a Template to Produce Surface-Enhanced Raman Scattering-Active Surfaces. *J. Phys. Chem. B* **2005**, *109*, 20186–20191.
52. Chan, S.; Kwon, S.; Koo, T. W.; Lee, L. P.; Berlin, A. A. Surface-Enhanced Raman Scattering of Small Molecules from Silver-Coated Silicon Nanopores. *Adv. Mater.* **2003**, *15*, 1595–1598.
53. Lin, H.; Mock, J.; Smith, D.; Gao, T.; Sailor, M. J. Surface-Enhanced Raman Scattering from Silver-Plated Porous Silicon. *J. Phys. Chem. B* **2004**, *108*, 11654–11659.
54. Kwon, K.; Lee, K. Y.; Lee, Y. W.; Kim, M.; Heo, J.; Ahn, S. J.; Han, S. W. Controlled Synthesis of Icosahedral Gold Nanoparticles and Their Surface-Enhanced Raman Scattering Property. *J. Phys. Chem. C* **2007**, *111*, 1161–1165.
55. Lahav, M.; Sehayek, T.; Vaskevich, A.; Rubinstein, I. Nanoparticle Nanotubes. *Angew. Chem., Int. Ed.* **2003**, *42*, 5575–5579.
56. Bruening, M. L.; Dotzauer, D. M.; Jain, P.; Baker, G. L. Creation of Functional Membranes Using Polyelectrolyte Multilayers and Polymer Brushes. *Langmuir* **2008**, *24*, 7663–7673.
57. Jiang, C.; Tsukruk, V. V. Freestanding Nanostructures *via* Layer-by-Layer Assembly. *Adv. Mater.* **2006**, *18*, 829–840.
58. Tsukruk, V. V. Assembly of Supramolecular Polymers in Ultrathin Films. *Prog. Polym. Sci.* **1997**, *22*, 247–311.